IEEE Access
Multidisciplinary ⋮ Rapid Review ⋮ Open Access Journal

Received February 28, 2020, accepted March 18, 2020, date of publication March 20, 2020, date of current version March 31, 2020.

Digital Object Identifier 10.1109/ACCESS.2020.2982317

Robust Oscillation Suppression Control of Electrified Powertrain System Considering Mechanical-Electric-Network Effects

WEI LI[1], WEI ZHU[1], XIAOYUAN ZHU[2,3], AND JINGANG GUO[2]

[1]School of Logistics Engineering, Shanghai Maritime University, Shanghai 201306, China
[2]Key Laboratory of Shanxi Province for Development and Application of New Transportation Energy, Chang'an University, Xi'an 710064, China
[3]Merchant Marine College, Shanghai Maritime University, Shanghai 201306, China

Corresponding author: Xiaoyuan Zhu (zhuxyc@gmail.com)

This work was supported in part by the Foundation of Key Laboratory of Shaanxi Province for Development and Application of New Transportation (Chang'an University) under Grant 300102229511, and in part by the National Natural Science Foundation of China under Grant 51605278.

ABSTRACT This paper works on the oscillation of electrified powertrain system in an integrated manner where combined mechanical-electric-network effects are all taking into consideration, and a robust oscillation controller is proposed to suppress the effects-caused oscillation and to maintain the system stability. An integrated model is developed in which driving motor, drivetrain and communication network are all included. Thus, torque ripples in the driving motor, nonlinear gear backlash as well as driveshaft flexibility in the drivetrain and network-induced delays that may cause powertrain system oscillation can be all considered. In order to dealing with the coupling effects of network-induced delays and event-driven manner of the controller nodes, a delay-free discrete model is further built via polytopic inclusion approach and system augmentation technique. An energy-to-peak performance based robust controller is proposed to ensure the torsional oscillation damping as well as vehicle speed tracking performance. During backlash mode, as the driving motor and the load are decoupled, a sliding mode compensator is further adopted to restrain the torsional oscillation. The stability of electrified powertrain control system is ensured by using Lyapunov theory, and the controller gain is obtained by solving a set of linear matrix inequalities (LMIs). Comparative simulation tests are carried out by using Matlab/Simulink in which a delicate controller area network (CAN) model is developed via SimEvent. The combined mechanical-electric-networked effects on torsional oscillation are demonstrated during the simulation tests, while the performance of the proposed controller is well verified.

INDEX TERMS Electrified powertrain, nonlinear gear backlash, network-induced delays, robust energy-to-peak controller, sliding mode compensator.

I. INTRODUCTION

The growing environmental pollution and the energy crisis urge the development of electric vehicles (EVs) for the emission reduction and the improvement of energy efficiency [1]–[3], what followed is a steadfast trend to the electrification of powertrain in recent years [4]. In order to reduce the efficiency loss, the electrified powertrain system trends to be compact with less damping parts and more simple mechanical structure. For most instances, the motor is directly connected to the gearbox of drivetrain without clutches or torque converter. Thus, the powertrain is becoming more sensitive to the oscillation caused by the driveshaft flexibility and the backlash [5], [6]. In order to optimize the powertrain system's oscillation damping performance, plenty of methods have been carried out. Comparing with passive approaches [7], [8], using controller design, which is classified as the active methods, demonstrates more superiority in cost, convenience and flexibility [9]. Liu *et al.* [10] provide an adaptive optimal shaking vibration controller for EVs, in which torsional vibration is considered without the effect of nonlinear gear backlash. While Lagerberg *et al.* [11] present nonlinear gear backlash estimators via the Kalman filtering theory for powertrain system with experimental validation. Zhang *et al.* [12] adopt the dual Kalman filter to estimate vehicle mass and half shaft torsional angle

The associate editor coordinating the review of this manuscript and approving it for publication was Huanqing Wang.

of driveline, which is further used to realize active vibration compensation. A mode switching based active controller for electrified powertrain system during regenerative braking is proposed in [13], which can effectively suppress driveline oscillation that caused by shaft flexibility and gear backlash.

It can be seen that most of the researches on powertrain oscillation are focusing on the mechanical features [14]. However, for the electrified powertrain system, torque wave of the driving motor with high ripples can also induce vibration and noise [15], [16]. Through theoretical modeling, analysis and experiments, Mao *et al.* [17] reveal and explain the high frequency vibration characteristics of electric wheel system brought by motor torque ripple excitation. Based on the effects of the rotor position error in the performance of field-oriented-control permanent magnet synchronous motor (PMSM) for EVs, Lara *et al.* [18] develop an extended and generalized PMSM model to evaluate the torque ripple. Arias *et al.* [19] develop a comprehensive discrete-time model to assess the field-oriented-controlled PMSM stability issues of EVs. Ye [20] propose a flux sliding mode observer in a sensorless control PMSM system to eliminate high-order harmonics, which can improve the performance of the PMSM drives.

Owning to the development of in-vehicle network and X-by-wire technologies, information in EVs is currently exchanged through CAN [21]. Electrification of EVs enhances delivery requirement, while the limitation of bandwidth restricts the requirement, which would inevitably induce time-varying delays [22], [23]. Jia *et al.* [24] propose an improved robust stability criterion to estimate the asymptotically stable for load frequency control system of EVs considering the inertia uncertainty and time-varying delays. Caruntu *et al.* [25] present the impact of network-induced delays to the oscillation of a vehicle drivetrain proposing a predictive controller to deal with time-varying delays. The impact of network-induced delays was taken into consideration in the lateral motion of vehicles [26] and the braking process of EVs [27]. The network-induced delays can deduct the control performance to the electrified powertrain system and may cause oscillation as well. The delays can be quantized and considered as uncertainties in a discrete-time system, which can be modeled as polytope type [28]. A backstepping-based quantized control algorithm is proposed in [29], which guarantees the robustness of non-strict-feedback systems. The quantizer's parameter of feedback control can be given based on the LMI technique [30].

Few works have been carried out to synthetically consider the combined mechanical-electric-network effects of the driving motor characteristics, network communication and drivetrain dynamics including driveshaft flexibility and gear backlash. Hence, it is necessary to develop a dynamic model of the electrified powertrain system, which can simultaneously reflect characteristics of motor and drivetrain system. Besides, the controller for the system should possess the robustness against the oscillation. Wang *et al.* [31] propose an observer-based adaptive backstepping decentralized controller for interconnected nonlinear systems suffering stochastic disturbances. Robust control method is effectively capable of handling the modeling error caused by system uncertainties and external disturbances [24], [32]. Chang *et al.* [33] propose a robust controller with H_∞ and energy to peak performance to deal with resilient control condition for lateral motion regulation of an intelligent vehicle, which can well compensate the fluctuation of controller. In this paper, the control performance is verified via Simulink, and the contributions of this study lie in four aspects:

(1) An integrated model of electrified powertrain system is established combining PMSM, drivetrain and CAN which can overall reflect the flux characteristics of PMSM, the nonlinear backlash, the flexibility of driveshaft in drivetrain and the CAN-induced delays.

(2) A delay-free discrete model is developed via system augmentation technique, where the CAN-induced time-varying delays are described via polytopic inclusion approach. And a robust controller basing on the energy-to-peak performance is designed to suppress the torsional oscillation of the electrified powertrain system against external disturbances.

(3) Due to the decoupled gear gap between the motor and the load in the backlash mode, a sliding mode compensator is further adopted to restrain the backlash-caused oscillation.

(4) A detailed CAN bus model is elaborated via SimEvent, by which the robustness of the proposed controller against the delays and the oscillation suppression control performance are verified.

The remainder of this paper is listed as follows: in Section II, problem formulation and dynamical modeling are presented. The robust controller and SMC compensator design are presented in Section III. Results and analysis of simulations via Simulink are shown in Section IV. Finally, section V summarizes this study to draw the conclusion of this paper.

II. PROBLEM FORMULATION

A. ARCHITECTURE OF THE PROPOSED ELECTRIFIED POWERTRAIN SYSTEM

The scheme of the proposed electrified powertrain system is shown in Fig.1 where the powertrain is mainly composed of a driving motor, a gearbox, a differential and drive shafts. The driving motor, which is a PMSM, is directly connected to the gearbox without clutch. Both the non-linear backlash in the gearbox and the torsional vibrations of the flexible driveshaft may cause the oscillation of the powertrain. The signals among the sensors, integrated controller unit (ICU) and driver are transmitted through the CAN network which is as the communication medium. The ICU receives the signal of the system states and the reference vehicle speed, and calculates the command voltage which is sent directly to the electrified powertrain system through CAN. The standard controller for a PMSM is a vector-based cascade arrangement

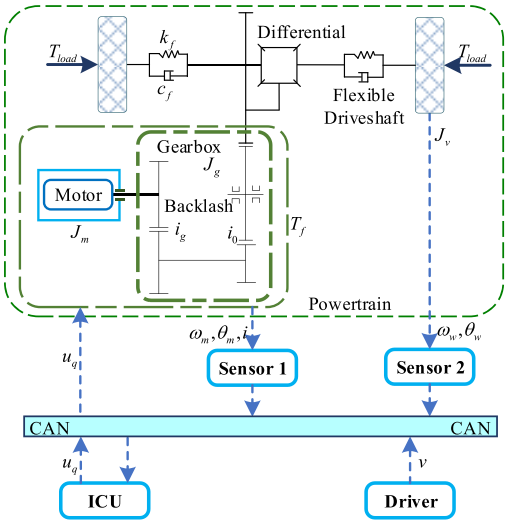

FIGURE 1. Scheme of the proposed electrified powertrain system.

[34], thus the signal of the current of the q axis is necessary. During the control process, the sensors are working in time-driven mode, while the ICU is working in event-driven mode.

B. DYNAMICAL MODELING OF DRIVING MOTOR

Based on the flux-linkage characteristics of the PMSM, dynamic model of the driving motor is described as

$$\begin{cases} \boldsymbol{u}_{3s} = \boldsymbol{R}\boldsymbol{i}_{3s} + \dot{\boldsymbol{\Phi}}_{3s} \\ \boldsymbol{\Phi}_{3s} = \boldsymbol{L}_{3s}\boldsymbol{i}_{3s} + \phi_f \cdot \boldsymbol{F}_{3s}(\theta_e) \\ T_m = \dfrac{1}{2} p_n \dfrac{\partial}{\partial \theta_m} \left(\boldsymbol{i}_{3s}^T \cdot \boldsymbol{\Phi}_{3s} \right) \end{cases} \tag{1}$$

where the variables are defined and calculated as

$$\begin{aligned} &\boldsymbol{i}_{3s} = \begin{bmatrix} i_A & i_B & i_C \end{bmatrix}^T, \quad \boldsymbol{\Phi}_{3s} = \begin{bmatrix} \phi_A & \phi_B & \phi_C \end{bmatrix}^T, \\ &\boldsymbol{u}_{3s} = \begin{bmatrix} u_A & u_B & u_C \end{bmatrix}^T, \\ &\boldsymbol{R} = diag\{R\ R\ R\}, \quad \boldsymbol{F}_{3s}(\theta_e) = \begin{bmatrix} \sin\theta_e \\ \sin(\theta_e - 2\pi/3) \\ \sin(\theta_e + 2\pi/3) \end{bmatrix}, \\ &\boldsymbol{L}_{3s} = L_{m3} \begin{bmatrix} 1 & \cos(2\pi/3) & \cos(4\pi/3) \\ \cos(2\pi/3) & 1 & \cos(2\pi/3) \\ \cos(4\pi/3) & \cos(2\pi/3) & 1 \end{bmatrix} + L_{l3}\boldsymbol{I} \end{aligned} \tag{2}$$

After taking the Clark and Park transformation, the model can be rewritten into

$$\begin{cases} u_d = Ri_d + L_d\dot{i}_d - n_p\omega_m L_q i_q \\ u_q = Ri_q + L_q\dot{i}_q + n_p\omega_m \left(L_d i_d + \phi_f \right) \\ T_m = \dfrac{3}{2} p_n i_q \left[i_d \left(L_d - L_q \right) + \phi_f \right] \end{cases} \tag{3}$$

where u is voltage, i is current and L is inductance in which the subscript $_d$ and $_q$ represent respectively the d axis and q axis. R is the resistance, n_p is the number of pole-pairs, ω_m is the motor speed, T_m is the output torque of the motor and ϕ_f is the flux of the permanent magnet.

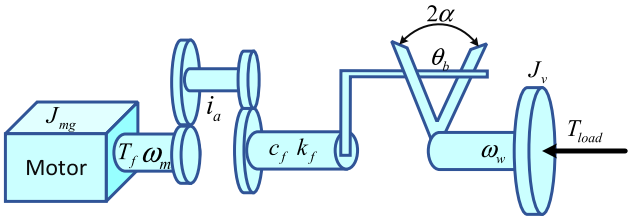

FIGURE 2. Dynamic model of drivetrain.

Consider the PMSM as a surface-mounted one, thus it can be obtained that $L = L_d = L_q$. Since it is under the vector-controlled mode, the d-axis current is tracked to zero, i.e. $i_d \to 0$, the dynamic model can be simplified as

$$\begin{cases} \dot{i}_q = -\dfrac{R}{L} i_q - \dfrac{n_p \phi_f}{L} \omega_m + \dfrac{1}{L} u_q \\ T_m = \dfrac{3}{2} n_p i_q \phi_f \end{cases} \tag{4}$$

C. DYNAMICAL MODELING OF DRIVETRAIN

As is shown in Fig.2, the backlash contributions throughout the powertrain are lumped together into one single backlash angle 2α, and the dynamics of the drivetrain can be obtained that

$$\begin{aligned} J_{mg}\omega_m^2 &= T_m - T_f/i_a - c_m\omega_m \\ J_v\dot{\omega}_w &= T_f - T_{load} \\ T_f &= k_f\left(\theta_m/i_a - \theta_w - \theta_b\right) + c_f\left(\omega_m/i_a - \omega_w - \dot{\theta}_b\right) \\ T_{load} &= T_{roll} + T_{grad} + T_{airinag} \\ T_{airdrag} &= c_a\omega_w \end{aligned} \tag{5}$$

where J_{mg} is the composite inertia of motor and gear box, ω_m and ω_w are the speed of motor and wheel respectively, while θ_m and θ_w are the output angles respectively. T_f is the driving torque in the driveshaft with stiffness factor k_f and damping coefficient c_f. i_a is the total transmission ratio of the powertrain, J_v is the equivalent inertia of the vehicle, T_{load} is the external load torque comprised of air drag $T_{airdrag}$, rolling torque T_{roll} and resistant torque T_{grad} due to the road grade. c_a is a linear approximation parameter for $T_{airdrag}$. Besides, the wheel slip is not considered in this model. θ_b is the position in the backlash with the gap size 2α, which non-linear model for the backlash position can be described as [35]

$$\dot{\theta}_b = \begin{cases} \max\left(0, \dot{\theta}_d + \dfrac{k_f}{c_f}\theta_s\right), & \theta_b = -\alpha \\ \dot{\theta}_d + \dfrac{k_f}{c_f}\theta_s, & |\theta_b| < \alpha \\ \min\left(0, \dot{\theta}_d + \dfrac{k_f}{c_f}\theta_s\right), & \theta_b = \alpha \end{cases} \tag{6}$$

where the angle position of θ_d and θ_s are defined as

$$\begin{aligned} \theta_d &:= \theta_m/i_a - \theta_w \\ \theta_s &:= \theta_d - \theta_b \end{aligned} \tag{7}$$

Thus, it can be obtained that the powertrain is switching between two linear modes, called contact mode (co) and backlash mode (bl), which are defined as

$$\begin{cases} co: & |\theta_b| = \alpha, \lambda\theta_b \geq 0 \\ bl: & |\theta_b| < \alpha \text{ or } (|\theta_b| = \alpha, \lambda\theta_b < 0) \end{cases}$$
$$\lambda := \dot{\theta}_d + \frac{k_f}{c_f}\theta_s \tag{8}$$

And the backlash mode in (6) can rewritten as

$$\dot{\theta}_b = \begin{cases} 0, & \text{mode}: co \\ \lambda, & \text{mode}: bl \end{cases} \tag{9}$$

Substituting (4) and (9) into (5), the motor torque turns into an intermediate variable instead of control input. Taking the errors of motor speed, wheel speed, axle wrap of the drivetrain and the q-axis current in the PMSM as the system states and the q-axis voltage as the control input, i.e.

$$\begin{aligned} x &= \left[\, \omega_m - \omega_m^* \;\; \omega_w - \omega_w^* \;\; \theta_s - \theta_s^* \;\; i_q - i_q^* \,\right]^T \\ u &= u_q \end{aligned} \tag{10}$$

The integrated state space model of electrified powertrain system can be described in two switching modes as

$$\begin{aligned} \dot{x} &= A_{co}x + B\left(u - u^*\right) + w \\ \dot{x} &= A_{bl}x + B\left(u - u^*\right) + w \end{aligned} \tag{11}$$

where the matrices are given by

$$A_{co} = \begin{bmatrix} -\frac{c_m}{J_{mg}} - \frac{c_f}{J_{mg}i_a^2} & \frac{c_f}{J_{mg}i_a} & -\frac{k_f}{J_{mg}i_a} & \frac{3n_p\phi_f}{2J_{mg}} \\ \frac{c_f}{J_v i_a} & -\frac{c_f + c_a}{J_v} & \frac{k_f}{J_v} & 0 \\ \frac{1}{i_a} & -1 & 0 & 0 \\ -\frac{n_p\phi_f}{L} & 0 & 0 & -\frac{R}{L} \end{bmatrix}$$
$$A_{bl} = \begin{bmatrix} -\frac{c_m}{J_{mg}} & 0 & 0 & \frac{3n_p\phi_f}{2J_{mg}} \\ 0 & -\frac{c_a}{J_v} & 0 & 0 \\ \frac{1}{i_a} & -1 & 0 & 0 \\ -\frac{n_p\phi_f}{L} & 0 & 0 & -\frac{R}{L} \end{bmatrix}, \quad B = \begin{bmatrix} 0 \\ 0 \\ 0 \\ \frac{1}{L} \end{bmatrix}$$
$$w = \begin{bmatrix} 0 & -\frac{T_{roll} + T_{grad}}{J_v} & 0 & 0 \end{bmatrix}^T \tag{12}$$

Based on the reference vehicle speed and the nominal load, other reference values can be all calculated for the controller. The disturbance term here mainly represent the characteristic of T_{roll} and T_{grad}, but it can also cover other external load disturbances and modelling errors, which will be handled via robust controller once and for all. The matric A_{bl} indicates that no torque is transmitted through the driveshaft in the backlash gap and that the motor and the load are decoupled. Thus, only in co-mode is the powertrain fully controllable, in which the CAN-induced delays are considered via modeling.

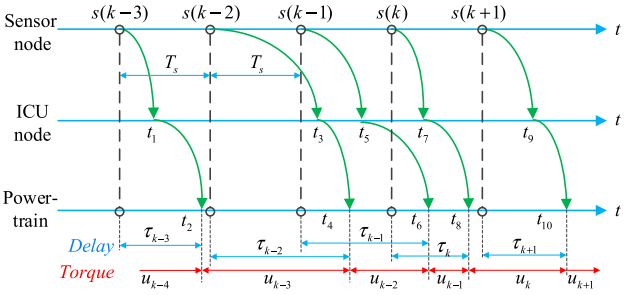

FIGURE 3. Signal transmission of electrified powertrain control system via CAN.

D. MODELING OF CAN-INDUCED DELAYS

As the signal transmission diagram shown in Fig.3, the time-driven sensors periodically deliver the data of states to the CAN under a fixed sampling period T_s, which are collected by event-driven ICU node from CAN. Then the ICU node sends the calculated voltage command to the powertrain via CAN. The signals will be transmitted twice through CAN to complete one closed loop. The ICU node and the powertrain are affected by the CAN-induced delays τ, which leads to the voltage command as time-varying value. The electrified powertrain system should be discretized because of the time-varying control period, which can present the effects of the delays as well, where the control period is described as

$$t \in [t_k + \tau_k, \quad t_{k+1} + \tau_{k+1}], \; t_k = kT_s \tag{13}$$

The signals are incapable of interlacing on the timeline [36], i.e. $\tau_k \geq \tau_{k-1} - T_s$. Thus, the CAN-induced delays can be described as

$$\tau_k = (\Upsilon + \upsilon)\, T_s, \Upsilon \in Z_+, \quad \upsilon \in R_{[0,1)} \tag{14}$$

The discretized electrified powertrain model under CAN-induced delays can be described as

$$\begin{aligned} x(k+1) \;=\; & A_1 x(k) + B_1 u(k) + E_1 w(k) \\ & + \Delta_{0,k}\left(u(k-1) - u(k)\right) \\ & + \Delta_{1,k}\left(u(k-2) - u(k-1)\right) \\ & + \cdots + \Delta_{\Upsilon,k}\left(u(k-\Upsilon-1) - u(k-\Upsilon)\right) \end{aligned}$$
$$\Delta_{i,k} := \begin{cases} 0, & \tau_{k-i} - iT_s \leq 0 \\ \int_0^{\tau_{k-i}-iT_s} e^{A_{co}(T_s-\theta)}d\theta B, & 0 \leq \tau_{k-i} - iT_s \leq T_s \\ \int_0^{T_s} e^{A_{co}(T_s-\theta)}d\theta B, & T_s \leq \tau_{k-i} - iT_s \end{cases}$$
$$A_1 := e^{A_{co}T_s}, \quad B_1 := \int_0^{T_s} e^{A_{co}(T_s-\theta)}d\theta B,$$
$$E_1 := \int_0^{T_s} e^{A_{co}(T_s-\theta)}d\theta E, \quad i = 0, 1 \cdots \Upsilon \tag{15}$$

The item $\Delta_{i,k}$ is highly nonlinear with the random value of delays and needs to be linearized. Taylor series expansion approach is adopted here making the system rewritten as

$$\begin{aligned} \Delta_{i,k} &= A_\tau x_\tau B, \quad x_\tau = \left[\, x \; x^2 \; \cdots \; x^h \,\right]^T \\ A_\tau &= e^{AT_s}\left[\, \frac{(-1)^2}{1!}A_{co}^0 \;\; \frac{(-1)^3}{2!}A_{co}^1 \;\; \cdots \;\; \frac{(-1)^{h+1}}{(h)!}A_{co}^{h-1} \,\right] \end{aligned} \tag{16}$$

where x_τ is the integral upper limit to system matrices $\Delta_{i,k}$, and h is the order of Taylor expansion.

The polytopic inclusions method is appropriate to describe the vertices of the CAN-induced delays [36], [37], and the $\Delta_{i,k}$ can be synthetically defined as

$$\begin{cases} \Delta_{i,k} = \sum_{m=0}^{1}\sum_{n=0}^{h} \eta_{i,m,n}(k) A_{\tau,m} x_{\tau,1,n} B, \\ \qquad\qquad \forall i = 0, 1, \cdots \Upsilon - 1 \\ \Delta_{i,k} = \sum_{m=0}^{1}\sum_{n=0}^{h} \eta_{i,m,n}(k) A_{\tau,m} x_{\tau,0,n} B, \quad i = \Upsilon \end{cases}$$
$$\sum_{m=0}^{1}\sum_{n=0}^{h} \eta_{i,m,n}(k) = 1 \tag{17}$$

where $\eta_{i,m,n}$ are the weighting coefficients. Besides, B_1 and E_1 can be defined similarly.

III. ROBUST OSCILLATION SUPPRESSION CONTROLLER DESIGN

A. ROBUST TORTIONAL VIBRATIONS CONTROLLER DESIGN

In order to present the CAN-induced time-varying delays into the states for the controller design, a delay-free model is established via system augmentation technique, the new states are defined as

$$\bar{x}(k) = \left[x^T(k)\ u^T(k-1)\ \cdots\ u^T(k-\Upsilon-1)\right]^T \tag{18}$$

then the discretized model in (17) can be rewritten as

$$\begin{aligned} \bar{x}(k+1) &= A_2\bar{x}(k) + B_2 u(k) + E_2 w(k) \\ A_2 &= \begin{bmatrix} A_1 & \Delta_{0,k} - \Delta_{1,k} & \cdots & \Delta_{\Upsilon-1,k} - \Delta_{\Upsilon,k} & \Delta_{\Upsilon,k} \\ 0 & 0 & \cdots & 0 & 0 \\ 0 & I & \cdots & 0 & 0 \\ \vdots & \vdots & \ddots & \vdots & \vdots \\ 0 & 0 & \cdots & I & 0 \end{bmatrix} \\ B_2 &= \left[B_1^T - \Delta_{0,k}^T \quad I \quad 0 \quad \cdots \quad 0\right]^T \\ E_2 &= \left[E_1^T \quad 0 \quad 0 \quad \cdots \quad 0\right]^T \end{aligned} \tag{19}$$

Based on the delay-free model in (19), the state-feedback controller structure is selected as

$$u(k) = K\bar{x}(k) \tag{20}$$

Thus, the closed-loop control system can be described as

$$\bar{x}(k+1) = (A_2 + B_2 K)\bar{x}(k) + E_2 w(k) \tag{21}$$

The torsional vibrations represented as the axle wrap will be inhibited during the EV's speed tracking. Thus, both the wheel speed error and axle wrap rate error are selected as the control outputs, which can be described as

$$Z_1 = C_1\bar{x}(k), \quad C_1 = \begin{bmatrix} 0\ I\ 0\ \underbrace{[0\ \cdots\ 0]}_{\Upsilon+1} \end{bmatrix}$$

$$Z_2 = C_2\bar{x}(k), \quad C_2 = \begin{bmatrix} \dfrac{I}{i_{g,n} i_f}\ -I\ 0\ \underbrace{[0\ \cdots\ 0]}_{\Upsilon+1} \end{bmatrix} \tag{22}$$

The energy-to-peak performance indexes are defined as

$$\|Z_1\|_\infty < \gamma_1 \|w\|_2, \quad \|Z_2\|_\infty < \gamma_2 \|w\|_2 \tag{23}$$

In order to prove the stability of the electrified powertrain control system, the Lyapunov function is defined as

$$V(k) = \bar{x}^T(k) P \bar{x}(k), \quad P > 0 \tag{24}$$

Without considering the disturbance w_k, the difference of Lyapunov function should satisfy following condition as

$$\begin{aligned} \Delta V(k) &= \bar{x}^T(k)\left(\Lambda^T P \Lambda - P\right)\bar{x}(k) < 0 \\ \Lambda &= A_2 + B_2 K \end{aligned} \tag{25}$$

Define a cost function to further ensure the robust of the electrified powertrain system and the matrix inequalities as

$$J = V(k) - \sum_{i=0}^{k-1} w^T(k) w(k) < 0 \ C_n^T C_n < \gamma_n^2 P, \quad n = 1, 2 \tag{26}$$

Furthermore, (26) is equivalent via Schur complement theory to

$$\begin{bmatrix} -P & P(A_2 + B_2 K) & PE_2 \\ * & -P & 0 \\ * & * & -I \end{bmatrix} < 0$$
$$\begin{bmatrix} -P & C_n^T \\ * & -\gamma_n^2 I \end{bmatrix} < 0, \quad n = 1, 2 \tag{27}$$

Removing the bilinear terms and taking the vertices of the convex polytope for the system matrices into consideration, both the stability and the energy-to-peak performance of the electrified powertrain system can be ensured through expanding the matrix as [36]

$$\begin{bmatrix} -P^{-1} & A_{2,i,j}P^{-1} + B_{2,i,j}Y & E_2 \\ * & -P^{-1} & 0 \\ * & * & -I \end{bmatrix} < 0$$
$$\begin{bmatrix} -P^{-1} & P^{-1}C_n^T \\ * & -\gamma_n^2 I \end{bmatrix} < 0, \quad n = 1, 2$$
$$\forall i = 1, 2; \quad j = 1, 2, \cdots, (h+1)^{\gamma+1} \tag{28}$$

The desired control gain K can be calculated via LMI toolbox as

$$K = YP \tag{29}$$

B. SLIDING MODE COMPENSATOR DESIGN FOR ELECTRIFIED POWERTRAIN IN BACKLASH MODE

During the speed tracking of the electrified powertrain system, the bl-mode is a transient comparing to co-mode. The robust controller is proved to be capable to maintain stability of the system in co-mode, thus a sliding mode compensator is further adopted in bl-mode as a compensator for the backlash because of its ability to address non-linearity and to achieve

a good performance and a fast response. The objective in bl-mode is to track the motor speed to the reference speed which is calculated via wheel speed in ICU. Thus, the error is defined as

$$e = \dot{\theta}_m / i_a - \dot{\theta}_w \tag{30}$$

The sliding mode surface with derivation and integration is defined as

$$S = \zeta e + \dot{e} + \xi \int e \tag{31}$$

where $\zeta > 0$ and $\xi > 0$ are two parameters that need to be designed, and it can be easily obtained that

$$\dot{S} = \zeta \dot{e} + \ddot{e} + \xi e \tag{32}$$

Make the reaching law an exponential one, which is

$$\dot{S} = -\alpha \operatorname{sgn} S - \beta S \tag{33}$$

where α and β ($\alpha > 0$ and $\beta > 0$) are two design parameters. The Lyapunov candidate is chosen as $V_{SM} = \frac{1}{2}S^2$, which yields

$$\dot{V}_{SM} = S\dot{S} = -\alpha |S| - \beta S^2 < 0 \tag{34}$$

The control voltage u_q can be obtained from (32) and (33) as

$$u = Hx_{SM} + \begin{bmatrix} -\alpha & -\beta \end{bmatrix} \begin{bmatrix} \operatorname{sgn} S \\ S \end{bmatrix} + d_{SM} \tag{35}$$

where the matrices are given by

$$\begin{aligned} x_{SM} &= \begin{bmatrix} \theta_m & \omega_m & \theta_w & \omega_w & i_q \end{bmatrix}^T \\ H &= \begin{bmatrix} -\dfrac{2J_{mg}L\xi}{3n_p\phi_f} \\ \dfrac{2c_mL\zeta}{3n_p\phi_f} - \dfrac{2c_m^2L}{3J_{mg}i_an_p\phi_f} + n_p\phi_f \\ \dfrac{2J_{mg}i_aL\xi}{3n_p\phi_f} \\ \dfrac{2J_{mg}i_aLc_a^2}{3J_v^2n_p\phi_f} - \dfrac{2J_{mg}i_aLc_a\zeta}{3J_vn_p\phi_f} \\ \dfrac{Lc_m}{J_{mg}i_a} + R - L\zeta \end{bmatrix}^T \\ d_{SM} &= \frac{2J_{mg}i_aL\,(c_a - J_v\zeta)}{3J_v^2n_p\phi_f}\left(T_{roll} + T_{grad}\right) \end{aligned} \tag{36}$$

Remark: The decoupling during the bl-mode oversets the robust controller to obtain the control gain K. For bl-mode is transient comparing with co-mode, it is reasonable that control gain K in bl-mode follows the one in co-mode. Meanwhile the sliding mode compensator is further adopted in bl-mode to make sure $e \to 0$ and thereby suppress the non-linear-backlash-caused oscillation. Thus, the proposed controller can work in co-mode as well as bl-mode.

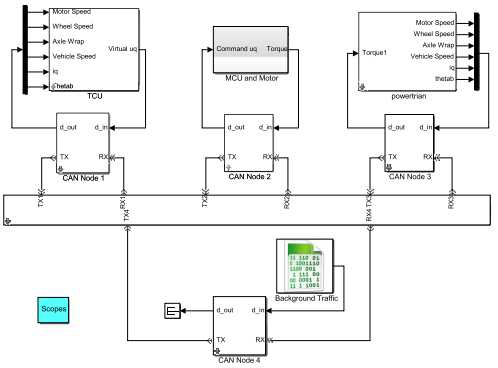

FIGURE 4. Simulation model of electrified powertrain control system over CAN.

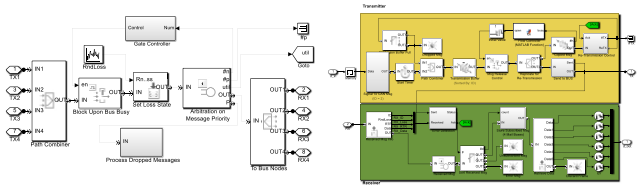

(a) (b)

FIGURE 5. Simulation model of CAN (a. CAN bus model and b. CAN node.

TABLE 1. Parameters of PMSM.

Parameters	Value	Unit
D/q-axis phase inductance (L)	0.35	mH
Phase resistance (R)	100	$m\Omega$
Flux linkage (ϕ_f)	0.07	Wb
Pole-pair (n_p)	5	-

IV. SIMULATION RESULTS AND ANALYSIS

The robustness and the control performance are verified via simulation in Matlab/Simulink. The model is established as shown in Fig.4 where a detailed CAN model is built via Matlab/SimEvent, which is composed of one bus model and four CAN node models. The details of the bus model and node model are shown in Fig.5. The controller works mainly in co-mode via the robust control gain K. Once the system turns into the bl-mode, the sliding mode compensator will be switched on to restrain the backlash and to suppress the oscillation of the electrified powertrain system.

The main parameters of the PMSM model are listed in Tab.1 [19], [38].

The main parameters of the drivetrain model are listed in Tab.2 [25].

The control gain is calculated via LMI toolbox, which is

$$K = \begin{bmatrix} -0.0023 & -93.9654 & -568.0545 \\ -0.0132 & -0.2216 & -0.1229 \end{bmatrix} \tag{37}$$

Parameters for the simulation are given by Tab.3.

TABLE 2. Parameters of drivetrain.

Parameters	Value	Unit
Inertia of motor and gearbox (J_{mg})	0.0162	$kg \cdot m^2$
Inertia of vehicle (J_v)	104.52	$kg \cdot m^2$
Motor damping (c_m)	0.15	-
Driveshaft damping (c_f)	42	-
Driveshaft stiffness (k_f)	6000	-
Approximation parameter (c_a)	2.7	-
Transmission ratio (i_a)	13.854	-

TABLE 3. Parameters for simulation.

Parameters	Value	Unit
Parameter ζ	0.5	-
Parameter ξ	200	-
Parameter α	55	-
Parameter β	6	-
Step size of solver	1	ms
Channel capacity	12000	bit/s
Loss probability	0.01%	-

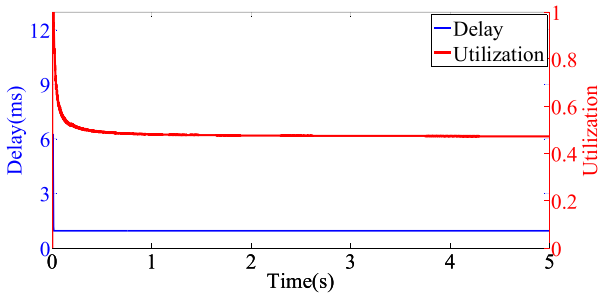

FIGURE 6. CAN performance under normal condition during acceleration test.

To make the result more convictive, two groups of simulation tests are conducted under with/without CAN-induced delays conditions, and a PI controller is adopted as a comparation to the proposed controller.

A. ACCELERATION TEST

Under this condition, the electrified powertrain system is controlled to acceleration process tracking to the vehicle speed of $50km/h$. The results are shown from Fig.6 to Fig.15.

It can be seen from Fig.6 that when there is no background traffic to cause delays, the utilization of the CAN bus is around 50% and there is only one solver step as $1ms$, which can be considered as no-induced-delay condition.

Under normal CAN condition, there are some slight oscillation caused by backlash shown in Fig.7, which PI controller

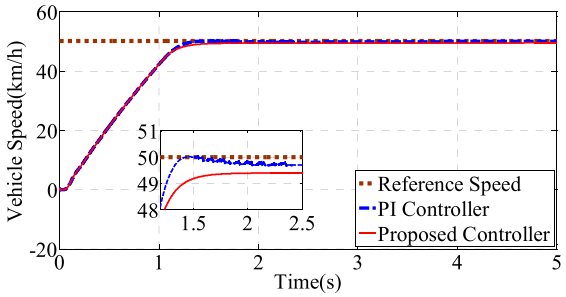

FIGURE 7. Vehicle speed tracking performance under normal CAN condition during acceleration test.

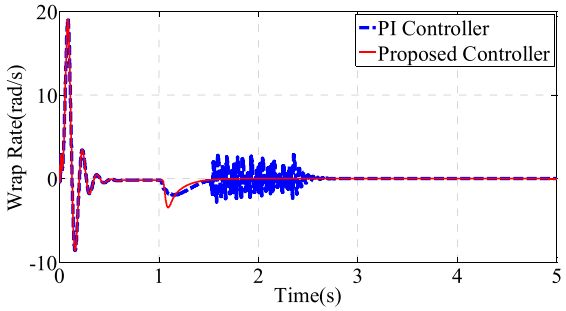

FIGURE 8. System oscillation performance under normal CAN condition during acceleration test.

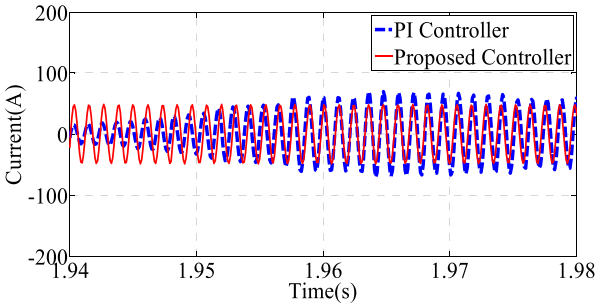

FIGURE 9. Phase A of the PMSM current under normal CAN condition during acceleration test.

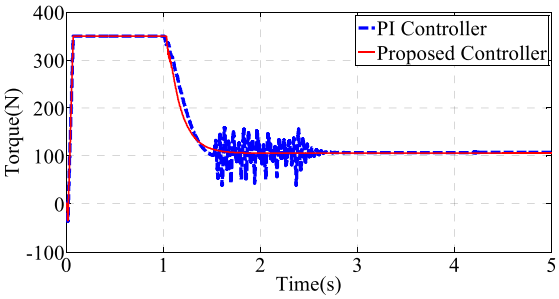

FIGURE 10. Driving torque of the electrified powertrain system under normal CAN condition during acceleration test.

cannot restrain, while it is acceptable for speed tracking and both the PI controller and proposed controller can track the reference vehicle speed and keep the system stable.

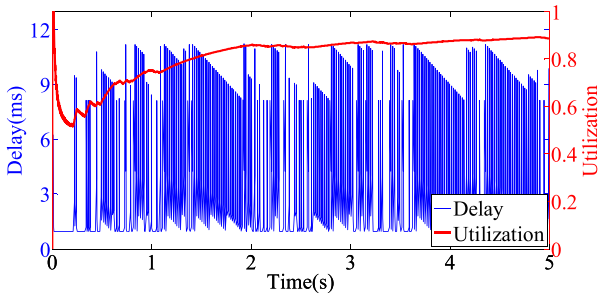

FIGURE 11. CAN performance under congestion condition during acceleration test.

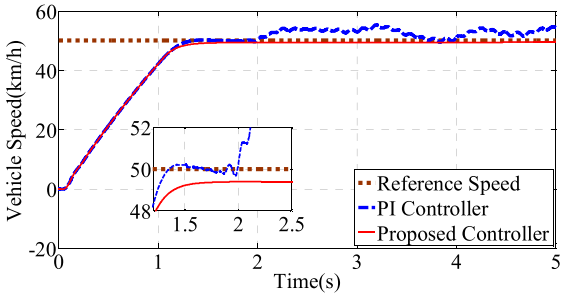

FIGURE 12. Vehicle peed tracking performance under congested CAN condition during acceleration test.

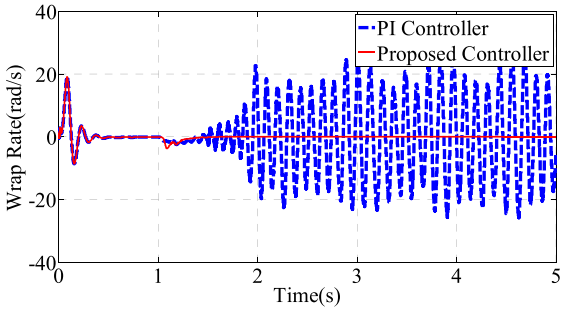

FIGURE 13. System oscillation performance under congested CAN condition during acceleration test.

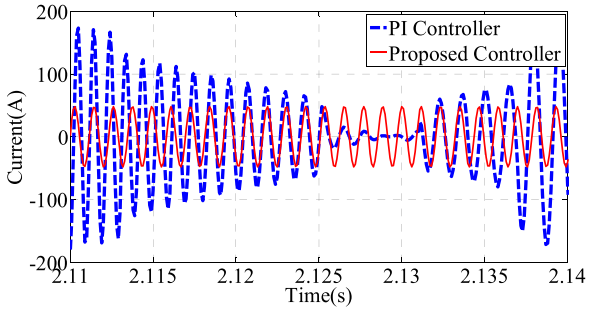

FIGURE 14. Phase A of the PMSM current under congested CAN condition during acceleration test.

It can be seen clearly from Fig.8 that the backlash can cause system oscillation which may impact the powertrain efficiency and service life of gears, and the proposed controller is able to compensate the backlash-caused oscillation.

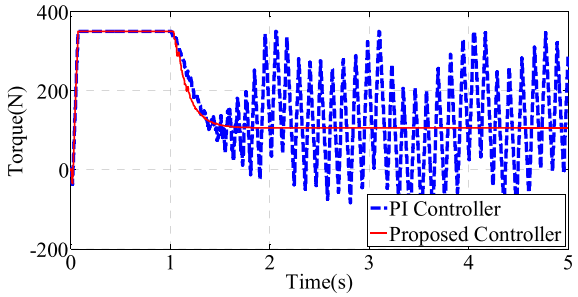

FIGURE 15. Driving torque of the electrified powertrain system under congested CAN condition during acceleration test.

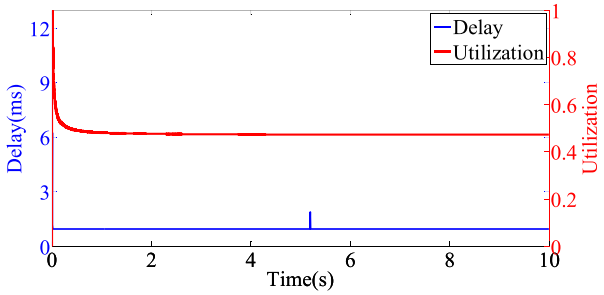

FIGURE 16. CAN performance under normal CAN condition during tip-in tip-out test.

It can be seen from Fig.9 and 10 that the backlash can affect the current of PMSM and driving torque, and the proposed controller can restrain the side effects of backlash.

It can be seen from Fig.11 that when the background traffic disturbance is added to cause time-varying delays, the utilization of the CAN bus is risen up over 80% and the CAN-induced delays are randomly around $9ms$, which is 9 times to the solver step.

It can be inferred from Fig.12 that the CAN-induced delays will deduct the speed tracking via PI controller in a certain extent, while the proposed controller remains the performance of speed tracking.

It is obvious that PI controller cannot suppress the torsional vibrations of driveshaft with induced delays shown in Fig.13, while the proposed controller can effectively suppress the torsional vibrations.

It can be seen from Fig.14 and 15 that torsional vibrations can impact the current of PMSM and its output torque, and the proposed controller instead of PI controller is competent to ensure the robust performance of the electrified powertrain system.

B. TIP-IN AND TIP-OUT TEST

Tip-in and tip-out test is conducted to further show the performance of proposed controller, in which the reference vehicle speed goes from $50km/h$ at the beginning and jumps into $30km/h$ at $4s$, then into $40km/h$ at $6.5s$, which can be seen in Fig.18 and 19. The results are shown from Fig16 to Fig23.

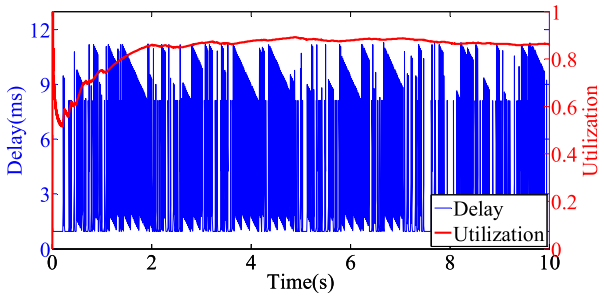

FIGURE 17. CAN performance under congested CAN condition during tip-in tip-out test.

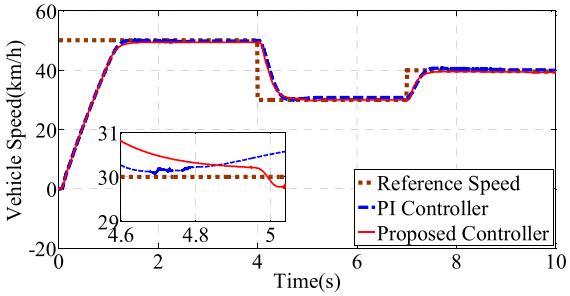

FIGURE 18. Vehicle speed tracking performance under normal CAN condition during tip-in tip-out test. **FIGURE 19.** Vehicle speed tracking performance under congested CAN condition during tip-in tip-out test.

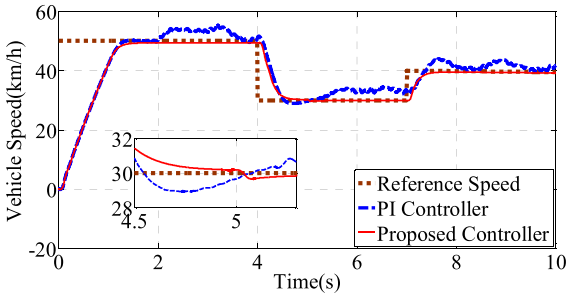

FIGURE 19. Vehicle speed tracking performance under congested CAN condition during tip-in tip-out test.

Fig.16 and 17 present the CAN utilization and delay under different CAN conditions, which are similar with Fig.6 and 11, except the simulation time is longer.

It can be inferred from Fig.18 and 19 that the PI controller cannot deal with the effect of the backlash and CAN-induced delays respectively. While the proposed controller can maintain the stability and robustness of the electrified powertrain system. There is a fluctuation in the performance of proposed controller at 5*s* due to the rigid switch of the sliding mode compensator, which may be further considered in the follow-up work to make switch smoother.

Comparing Fig.20 and 21, both the two controllers can deal with the torsional vibrations under normal CAN condition, while PI controller fails with the delays. Moreover, the PI controller has no capability to restrain the backlash, while the proposed controller can suppress the system oscillation

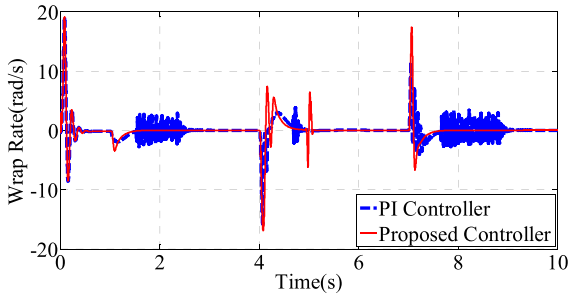

FIGURE 20. System oscillation performance under normal CAN condition during tip-in tip-out test.

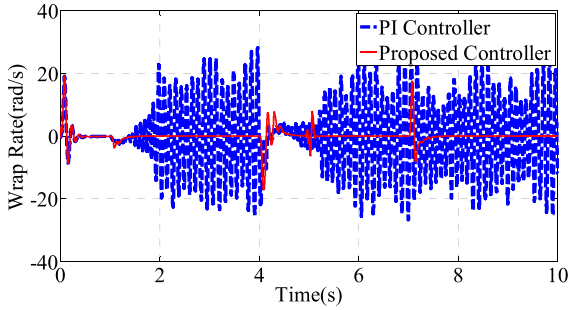

FIGURE 21. System oscillation performance under congested CAN condition during tip-in tip-out test.

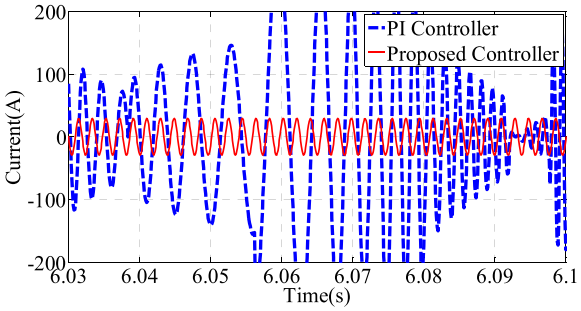

FIGURE 22. Phase A of the PMSM current under congested CAN condition during tip-in tip-out test.

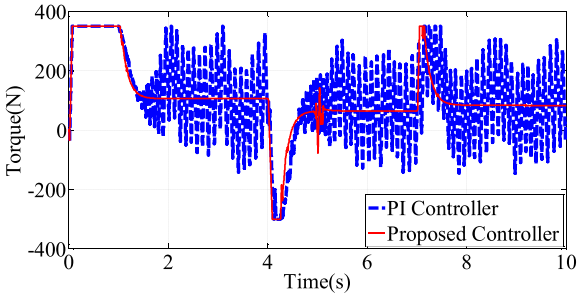

FIGURE 23. Driving torque of the electrified powertrain system under congested CAN condition during tip-in tip-out test.

composed with backlash and torsional vibrations even against the CAN-induced time-varying delays.

Fig.22 and 23 can further present that system oscillation can impact the current and torque of PMSM as well as the

rigid switch. The proposed controller can generally meet the controller objective for the electrified powertrain system, and it is reasonable to set the saturation of the driving torque as $[-300, 350]\,N \cdot m$.

V. CONCLUSION

In this paper, a robust oscillation suppression controller is designed for electrified powertrain system considering combined mechanical-electric-network effects. An integrated model is developed including driving motor, drivetrain and communication network so that torque ripples in the driving motor, nonlinear gear backlash as well as driveshaft flexibility in the drivetrain and network-induced delays that may cause powertrain system oscillation can be all taken into consideration. The polytopic inclusion approach and system augmentation technique are adopted to further develop a delay-free discrete model that can theoretically deal with the coupling effects of network-induced delays and event-driven manner of controller nodes. An energy-to-peak performance based robust controller is proposed to suppress the torsional oscillation as well as to maintain the vehicle speed tracking performance. Since the driving motor and the load are decoupled in the backlash mode, a sliding mode compensator is further adopted to restrain the torsional oscillation. The stability of the electrified powertrain control system is proved through Lyapunov theory and is validated through acceleration and tip-in tip-out tests. The combined mechanical-electric-networked effects on torsional oscillation are demonstrated during the comparative simulation tests, while the performance of the proposed controller is well verified.

REFERENCES

[1] M. V. Faria, R. A. Varella, G. O. Duarte, T. L. Farias, and P. C. Baptista, "Engine cold start analysis using naturalistic driving data: City level impacts on local pollutants emissions and energy consumption," *Sci. Total Environ.*, vol. 630, pp. 544–559, Jul. 2018.

[2] P. Spanoudakis, N. C. Tsourveloudis, L. Doitsidis, and E. S. Karapidakis, "Experimental research of transmissions on electric vehicles' energy consumption," *Energies*, vol. 12, no. 3, p. 388, 2019.

[3] J. Lian, L. Li, X. Liu, H. Huang, Y. Zhou, and H. Han, "Research on adaptive control strategy optimization of hybrid electric vehicle," *J. Intell. Fuzzy Syst.*, vol. 30, no. 5, pp. 2581–2592, Apr. 2016.

[4] X. Zhu, F. Meng, H. Du, and H. R. Karimi, "Advanced powertrain dynamic modelling and control for electrified vehicles," *Adv. Mech. Eng.*, vol. 10, no. 10, Oct. 2018, Art. no. 168781401880560.

[5] P. Templin and B. Egardt, "A powertrain LQR-torque compensator with backlash handling," *Oil Gas Sci. Technol.-Revue d'IFP Energies nouvelles*, vol. 66, no. 4, pp. 645–654, Jul. 2011.

[6] Y. Liu, X. Zhu, H. Zhang, and M. Basin, "Improved robust speed tracking controller design for an integrated motor-transmission powertrain system over controller area network," *IEEE/ASME Trans. Mechatronics*, vol. 23, no. 3, pp. 1404–1414, Jun. 2018.

[7] F. Wang, J. Zhang, X. Xu, Y. Cai, Z. Zhou, and X. Sun, "New method for power allocation of multi-power sources considering speed-up transient vibration of planetary power-split HEVs driveline system," *Mech. Syst. Signal Process.*, vol. 128, pp. 1–18, Aug. 2019.

[8] F. Wang, J. Zhang, X. Xu, Y. Cai, Z. Zhou, and X. Sun, "New teeth surface and back (TSB) modification method for transient torsional vibration suppression of planetary gear powertrain for an electric vehicle," *Mechanism Mach. Theory*, vol. 140, pp. 520–537, Oct. 2019.

[9] P. D. Walker and N. Zhang, "Active damping of transient vibration in dual clutch transmission equipped powertrains: A comparison of conventional and hybrid electric vehicles," *Mechanism Mach. Theory*, vol. 77, pp. 1–12, Jul. 2014.

[10] W. Liu, H. He, F. Sun, and H. Wang, "Optimal design of adaptive shaking vibration control for electric vehicles," *Vehicle Syst. Dyn.*, vol. 57, no. 1, pp. 134–159, Jan. 2019.

[11] A. Lagerberg and B. Egardt, "Backlash estimation with application to automotive powertrains," *IEEE Trans. Control Syst. Technol.*, vol. 15, no. 3, pp. 483–493, May 2007.

[12] J. Zhang, B. Chai, and X. Lu, "Active oscillation control of electric vehicles with two-speed transmission considering nonlinear backlash," *Proc. Inst. Mech. Eng., K, J. Multi-Body Dyn.*, vol. 234, no. 1, pp. 116–133, Mar. 2020.

[13] C. Lv, J. Zhang, Y. Li, and Y. Yuan, "Mode-switching-based active control of a powertrain system with non-linear backlash and flexibility for an electric vehicle during regenerative deceleration," *Proc. Inst. Mech. Eng., D, J. Automobile Eng.*, vol. 229, no. 11, pp. 1429–1442, Sep. 2015.

[14] X. Tang, X. Hu, W. Yang, and H. Yu, "Novel torsional vibration modeling and assessment of a power-split hybrid electric vehicle equipped with a dual-mass flywheel," *IEEE Trans. Veh. Technol.*, vol. 67, no. 3, pp. 1990–2000, Mar. 2018.

[15] D. Fodorean, M. M. Sarrazin, C. S. Martis, J. Anthonis, and H. Van der Auweraer, "Electromagnetic and structural analysis for a surface-mounted PMSM used for light-EV," *IEEE Trans. Ind. Appl.*, vol. 52, no. 4, pp. 2892–2899, Jul. 2016.

[16] X. Chen, S. Han, J. Li, T. Deng, and H. Wei, "Investigation of electromechanical coupling lateral/torsional vibration in a high-speed rotating continuous flexible shaft of PMSM," *Appl. Math. Model.*, vol. 77, pp. 506–521, Jan. 2020.

[17] Y. Mao, S. Zuo, X. Wu, and X. Duan, "High frequency vibration characteristics of electric wheel system under in-wheel motor torque ripple," *J. Sound Vibrat.*, vol. 400, pp. 442–456, Jul. 2017.

[18] J. Lara, J. Xu, and A. Chandra, "Effects of rotor position error in the performance of field-oriented-controlled PMSM drives for electric vehicle traction applications," *IEEE Trans. Ind. Electron.*, vol. 63, no. 8, pp. 4738–4751, Aug. 2016.

[19] A. Arias, E. Ibarra, E. Trancho, R. Griñó, I. Kortabarria, and J. Caum, "Comprehensive high speed automotive SM-PMSM torque control stability analysis including novel control approach," *Int. J. Electr. Power Energy Syst.*, vol. 109, pp. 423–433, Jul. 2019.

[20] S. Ye, "Design and performance analysis of an iterative flux sliding-mode observer for the sensorless control of PMSM drives," *ISA Trans.*, vol. 94, pp. 255–264, Nov. 2019.

[21] Z. Shuai, H. Zhang, J. Wang, J. Li, and M. Ouyang, "Combined AFS and DYC control of four-wheel-independent-drive electric vehicles over CAN network with time-varying delays," *IEEE Trans. Veh. Technol.*, vol. 63, no. 2, pp. 591–602, Feb. 2014.

[22] X. Zhu, H. Zhang, B. Yang, and G. Zhang, "Cloud-based shaft torque estimation for electric vehicle equipped with integrated motor-transmission system," *Mech. Syst. Signal Process.*, vol. 99, pp. 647–660, Jan. 2018.

[23] W. Li, W. Zhu, X. Zhu, Y. Xu, J. Yang, and Z. Li, "Torsional oscillations control of integrated motor-transmission system over controller area network," *IEEE Access*, vol. 8, pp. 4397–4407, 2020.

[24] H. Jia, X. Li, Y. Mu, C. Xu, Y. Jiang, X. Yu, J. Wu, and C. Dong, "Coordinated control for EV aggregators and power plants in frequency regulation considering time-varying delays," *Appl. Energy*, vol. 210, pp. 1363–1376, Jan. 2018.

[25] C. F. Caruntu, M. Lazar, R. H. Gielen, P. P. J. van den Bosch, and S. Di Cairano, "Lyapunov based predictive control of vehicle drivetrains over CAN," *Control Eng. Pract.*, vol. 21, no. 12, pp. 1884–1898, Dec. 2013.

[26] X. Zhu, H. Zhang, J. Wang, and Z. Fang, "Robust lateral motion control of electric ground vehicles with random network-induced delays," *IEEE Trans. Veh. Technol.*, vol. 64, no. 11, pp. 4985–4995, Nov. 2015.

[27] W. Li, W. Zhu, X. Zhu, and J. Guo, "Two-Time-Scale braking controller design with sliding mode for electric vehicles over CAN," *IEEE Access*, vol. 7, pp. 128086–128096, 2019.

[28] X.-H. Chang, R. Huang, and J. H. Park, "Robust guaranteed cost control under digital communication channels," *IEEE Trans. Ind. Informat.*, vol. 16, no. 1, pp. 319–327, Jan. 2020.

[29] H. Wang, P. X. Liu, X. Xie, X. Liu, T. Hayat, and F. E. Alsaadi, "Adaptive fuzzy asymptotical tracking control of nonlinear systems with unmodeled dynamics and quantized actuator," *Inf. Sci.*, early access, Apr. 3, 2018. [Online]. Available: https://www.sciencedirect.com/science/article/pii/S002002551830272X, doi: 10.1016/j.ins.2018.04.011.

[30] X.-H. Chang, R. Huang, H. Wang, and L. Liu, "Robust design strategy of quantized feedback control," *IEEE Trans. Circuits Syst. II, Exp. Briefs*, early access, Jun. 12, 2019, doi: 10.1109/TCSII.2019.2922311.

[31] H. Wang, P. X. Liu, J. Bao, X.-J. Xie, and S. Li, "Adaptive neural output-feedback decentralized control for large-scale nonlinear systems with stochastic disturbances," *IEEE Trans. Neural Netw. Learn. Syst.*, vol. 31, no. 3, pp. 972–983, Mar. 2020, doi: 10.1109/TNNLS.2019.2912082.
[32] L. Ma, X. Huo, X. Zhao, B. Niu, and G. Zong, "Adaptive neural control for switched nonlinear systems with unknown backlash-like hysteresis and output dead-zone," *Neurocomputing*, vol. 357, pp. 203–214, Sep. 2019.
[33] X.-H. Chang, Y. Liu, and M. Shen, "Resilient control design for lateral motion regulation of intelligent vehicle," *IEEE/ASME Trans. Mechatronics*, vol. 24, no. 6, pp. 2488–2497, Dec. 2019.
[34] S. Chai, L. Wang, and E. Rogers, "Model predictive control of a permanent magnet synchronous motor with experimental validation," *Control Eng. Pract.*, vol. 21, no. 11, pp. 1584–1593, Nov. 2013.
[35] A. Lagerberg and B. Egardt, "Estimation of backlash in automotive powertrains—An experimental validation," *IFAC Proc. Volumes*, vol. 37, no. 22, pp. 47–52, vol. 2004.
[36] X. Zhu, H. Zhang, D. Cao, and Z. Fang, "Robust control of integrated motor-transmission powertrain system over controller area network for automotive applications," *Mech. Syst. Signal Process.*, vols. 58–59, pp. 15–28, Jun. 2015.
[37] X. Zhu and W. Li, "Takagi–Sugeno fuzzy model based shaft torque estimation for integrated motor–transmission system," *ISA Trans.*, vol. 93, pp. 14–22, Oct. 2019.
[38] L. Harnefors and H.-P. Nee, "Model-based current control of AC machines using the internal model control method," *IEEE Trans. Ind. Appl.*, vol. 34, no. 1, pp. 133–141, Jan./Feb. 1998.

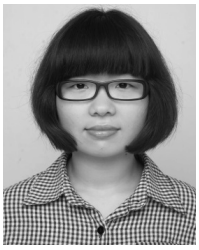

WEI LI received the B.E. and Ph.D. degrees in mechanical engineering from Northwestern Polytechnical University, Xi'an, China, in 2009 and 2015, respectively. From 2012 to 2014, she was a Visiting Scholar with the Department of Mechanical Engineering, Northwestern University, Evanston, IL, USA. She is currently with the School of Logistical Engineering, Shanghai Maritime University, China. Her current research interests include reliability engineering and mechatronic system control.

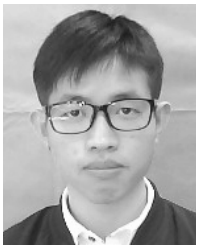

WEI ZHU received the B.E. degree in mechanical engineering from Shanghai Dianji University, in 2018. He is currently pursuing the M.S. degree with Shanghai Maritime University, China. His research interest includes vehicle system and control.

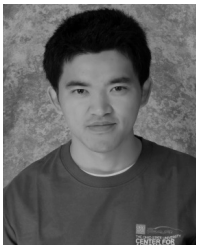

XIAOYUAN ZHU received the B.E. and Ph.D. degrees in mechanical engineering from Northwestern Polytechnical University, Xi'an, China, in 2009 and 2015, respectively. From 2012 to 2014, he was a Visiting Scholar with the Department of Mechanical and Aerospace Engineering, The Ohio State University, Columbus, OH, USA. He is currently with the Merchant Marine College, Shanghai Maritime University, China. His current research interests include e-drive system and control, automated driving, and wind and wave energy. He serves as a Guest Editor for *Advances in Mechanical Engineering* and an Outstanding Reviewer for many distinguished journals, including *Mechanical System and Signal Processing*, *ISA Transactions*, *Mechanism and Machine Theory*, and *Neurocomputing*.

JINGANG GUO received the Ph.D. degree from Xi'an Jiaotong University, in 2010. From 2013 to 2014, he was a Visiting Scholar with the Department of Mechanical and Aerospace Engineering, The Ohio State University, Columbus, OH, USA. He is currently an Associate Professor with the School of Automobile, Chang'an University, China. His research interests include optimization of electric propulsion systems and control of brake systems.